Catalysis Letters
https://doi.org/10.1007/s10562-019-02969-3

Promoter Effects on Catalyst Selectivity and Stability for Propylene Partial Oxidation to Acrolein

Patricia Anne Ignacio-de Leon[1] · Magali Ferrandon[2] · Louisa M. Savereide[3] · Scott L. Nauert[3] · Jorge Moncada[4] · Rachel Klet[2] · Karena Chapman[5] · Massimiliano Delferro[2] · Jeffrey Camacho-Bunquin[2] · Carlos A. Carrero[4] · Justin M. Notestein[3] · SonBinh Nguyen[6]

Received: 1 August 2019 / Accepted: 14 September 2019

Abstract

Highly dispersed silica-supported CuO_x/SiO_2 catalysts were synthesized via solution-phase deposition and studied for their activity, selectivity, and stability in catalyzing the selective oxidation of propylene to acrolein. Strategies for ensuring high metal dispersion included controlling the surface density of silanols (via covalent silanol-capping) or by pre-installing different "promoter" transition metals at submonolayer coverages. A comparison of the effect of first row transition metal promoters showed that V and Cr significantly boost catalyst performance and stabilize CuO_x sites against aggregation.

Graphic Abstract

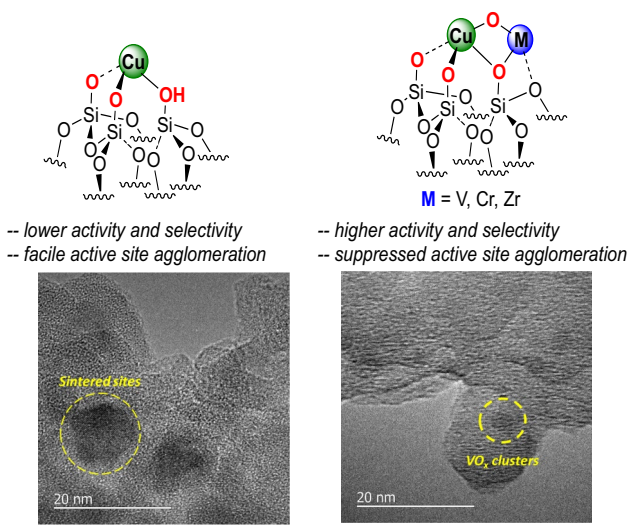

Keywords Acrolein · Copper · Oxidation · Promoter · Propylene

1 Introduction

The catalytic partial oxidation of propylene to acrolein has become one of the most studied reactions in hydrocarbon oxidation [1–6]. Various catalyst design elements have been investigated in the design of supported catalysts for selective partial oxidation of propylene to acrolein. Specifically, the effects of active site and oxide dispersion,

Electronic supplementary material The online version of this article (https://doi.org/10.1007/s10562-019-02969-3) contains supplementary material, which is available to authorized users.

✉ Magali Ferrandon
Ferrandon@anl.gov

Extended author information available on the last page of the article

Published online: 05 October 2019

presence of promoter ions and nature of solid supports (i.e., acidity and basicity) have been studied in the development of catalytic materials that activate C–H bonds and sequentially mediate oxygen atom transfer to form C–O bonds [7]. Despite the breadth of catalytic systems developed and studied for this reaction, gains in performance and fundamental understanding are still needed [8]. Heterogeneous catalysts for propylene-to-acrolein oxidation include monometallic materials like CuO_x–SiO_2 and multimetallic/multicomponent materials like promoted bismuth molybdates [9–11]. The relative compositional simplicity of the CuO_x/SiO_2 systems renders them more amenable to structure–activity correlation studies. Recent studies on CuO_x/SiO_2-catalyzed propylene oxidation to acrolein suggest that site dispersion is key to achieve high selectivity to acrolein; Schüth and coworkers [8] reported that highly diluted CuO_x on SiO_2 afforded higher selectivity to acrolein and reduced combustion to carbon oxides and C1–C2 cracking products. Site dispersion has also been shown to be important in other transition metal-based oxidation catalysts; sub-monolayer VO_x–SiO_2 enhanced propylene oxidation selectivity to oxygenates, particularly acrolein [12].

High active site dispersion could be achieved via two general synthetic strategies. The first approach involves the purposeful decrease in SiO_2 surface hydroxyl concentration via thermal treatment or covalent surface modification (e.g., –$SiMe_3$ capping), while the second approach involves modifying oxide surfaces with cationic 'anchors' that stabilize highly dispersed catalytic sites [13–15]. In the latter approach, the cations can also act as catalyst promoters [16–19]. The promoter effect was thought to be responsible for the enhanced oxygenates selectivity of Fe catalysts [20–22]. Enhancement in CuO_x/SiO_2 selectivity to acrolein was observed in the presence of Au promoters; Au was proposed to stabilize low-valent Cu^{1+} species which are more selective to oxygenate formation (e.g., acrolein) [18]. Similarly, the effects of transition metal promoter cations on the activity and selectivity of supported CuO_x systems for hydrocarbon partial oxidation have been demonstrated in the use of redox-active V [23–26] and Cr [27–30] sites. One limitation of prior studies on these promotion effects is that initial surface densities are typically high, presenting a range of surface structures and a relatively low number of the isolated sites proposed to be the most selective.

In this paper, we first investigate how these two synthetic strategies (TMS-capped SiO_2 and promoter-modified SiO_2) can be employed to increase the dispersion and stabilization of active sites for propylene oxidation, especially at very low surface coverages where statistical isolation is expected, at least for the initial catalyst state. Then we focus on a few promising promoters which lead to higher yield and higher stabilisation of active sites.

2 Experimental

2.1 Preparation of Trimethylsilyl-Capped SiO_2

Commercially available mesoporous silica support (Selecto Scientific, 30–200 µm size, pore size ca. 6 nm, surface area 520 m^2/g) was used (Fig. S1a, see Supporting Information). To 20 g SiO_2 in 250 mL hexane in a 500-mL round bottom flask, 15 mL of hexamethyldisilane (HMDS, Me_3Si-$SiMe_3$) was added with stirring. The mixture was refluxed overnight, and the solids filtered after allowing to cool to room temperature. After rinsing with three 200-mL portions of hexane, the solids were dried *in vacuo* at 120 °C for complete removal of any unreacted and by-product silanes and solvent. Thermal gravimetric analyses (TGA) of dried solids indicated the presence of a trimethylsilyl groups at a coverage of ca. 0.6 moieties per nm^2, thus reducing silanol surface density to about 1.3 SiOH/nm^2 (Fig. S2, Table S1). The trimethylsilyl-capped SiO_2 is labelled TMS-SiO_2.

2.2 Preparation of M/TMS-SiO_2 (M = Fe, Co, Cu)

Metal ions known for their catalytic oxidation activity (specifically Fe, Co and Cu) were installed via grafting of molecular precursors on TMS-SiO_2, using molecular *bis*(hexamethyldisilazido) iron(II), *bis*(hexamethyldisilizado)cobalt(II) and *bis*(dimethylamino-2-propoxy)copper(II) precursors in toluene at room temperature for 24 h. Two loadings (0.1 and 1.0 metal atoms/nm^2) of Cu, Fe, and Co supported on TMS-SiO_2 were chosen.

2.3 Preparation of M-SiO_2 Supports (M = V, Cr, Zn, Co, Zr)

SiO_2 treated at 200 °C under vacuum overnight was chosen as support. The 2.5 wt% VO_x on SiO_2 and 0.7 wt% CrO_x on SiO_2 supports were synthesized via incipient wetness technique following published methods from an aqueous solution of ammonium metavanadate (NH_4VO_3) mixed with oxalic acid ($H_2C_2O_4$) [31], and a methanolic solution of chromium(III) nitrate nona-hydrate ($Cr(NO_3)_3{\cdot}9H_2O$), respectively [32]. The 8.3 wt% Zn^{2+}/SiO_2 and 9.5 wt% Co^{2+}/SiO_2 supports were prepared by strong electrostatic attraction (SEA), employing literature methods from aqueous solutions at pH 11 of zinc(II) nitrate hexa-hydrate [33] ($Zn(NO_3)_2{\cdot}6H_2O$) and hexamminecobalt(III) chloride [34] ($Co(NH_3)_6Cl_3$), respectively. In addition, 3.9 wt% Zr^{4+}/SiO_2 support was prepared via solution-phase deposition of *tetrakis*(isopropoxy)zirconium(IV). The samples were

calcined at various temperatures (See supporting information for detailed synthesis procedures).

2.4 Deposition of Copper onto SiO_2 and M-SiO_2 Supports via High-Throughput Synthesis

A protocol was developed for high-throughput, automated synthesis of catalysts that included support and solution dispensing, stirring/shaking and washing. Using this methodology, a wide range of copper loadings (nominally 0.05 to 0.25 metal atom/nm^2), using bis(dimethylamino-2-propoxy)copper(II) as precursor in toluene, was deposited on SiO_2 pre-treated at 200 °C under vacuum overnight and on M-SiO_2 (M = V, Cr, Zn, Co, Zr) supports. There was no further treatment after deposition. Details can be found in SI.

2.5 Catalyst Characterization

A JEOL JEM-2100F transmission electron microscope (TEM) was used for all bright field imaging at 200 kV. Samples were prepared by dispersing solids in ethanol via sonication for 30 s. Colloidal suspensions were drop cast onto either Mo grids or lacey C on Ni grids (300 mesh) from Electron Microscopy Sciences at Argonne National Laboratory. TEM was used to probe for the presence of metal clusters on the supports; however, it should be noted that sample preparation for TEM analyses (sonication in ethanol) as well as imaging conditions (a 200 kV electron beam) could change material composition in situ (e.g., metal agglomeration). Diffuse reflectance UV–Vis spectra were collected with a Shimadzu UV-3600 spectrophotometer equipped with a Harrick Praying Mantis diffuse reflectance accessory. Polytetrafluoroethylene was used as the baseline white standard, and reflectance data were transformed to pseudo-absorbance using the Kubelka–Munk function, $F(R_\infty)$. Elemental analysis was performed using a Thermo iCap7600 ICP-OES instrument. Approximately 30 mg of sample was digested in 1 mL of HF and subsequently diluted to 11 mL with a 0.9 wt% HNO_3 aqueous solution. Standards of known concentration were prepared to quantify the samples' metal content. Raman spectroscopy studies were performed using a Renishaw InVia Qontor Raman Spectrometer equipped with 785, 532, and 405 nm solid-state lasers, ×5, ×20, ×50, and ×100 objectives, and a MS 20 Encoded Stage. All measurements used a 785 nm laser and 1200 L mm^{-1} grating and were taken with a range of 200–1500 cm^{-1} using a 50× long distance objective, 30 s of exposure time, and six accumulations under ambient conditions. The laser power used was tuned to get the maximum Raman spectra intensities without damaging the different metal oxide supported catalysts. H_2-TPR studies were carried out in an Altamira (AMI-100) system. A mixture of 3%H_2/N_2 at atmospheric pressure was used. Samples of 25 mg were loaded into a quartz U-tube reactor and calcined in air at 500 °C for 15 min. The samples were then cooled down to 30 °C in Ar. The H_2-TPR profiles were obtained by flowing H_2/Ar mixture at 50 mL/min from 30 to 700 °C at 10 °C/min. The hydrogen consumption was monitored quantitatively using a thermal conducutivity detector. High energy X-ray total scattering data suitable for pair distribution function (PDF) analysis were collected at beamline 11-ID-B of the Advanced Photon Source at Argonne National Laboratory. Data were collected in 3–5 min exposures using an amorphous-silicon based area detector at an X-ray wavelength of ~ 0.211 Å. The images were reduced to one-dimensional diffraction patterns within GSAS-II and PDFs calculated within PDFgetX2 and XPDFsuite, following subtraction of the background. Differential PDFs were calculated by subtracting the PDF measured for the support from that measured with the catalytic functionalization.

2.6 High-Throughput Catalyst Testing

High-throughput catalyst testing was carried out to identify optimum conditions (temperature, propylene to oxidant ratio) for further testing and to screen a large number of catalysts. Propylene oxidation to acrolein was performed in a 16 fixed bed reactor system (Flowrence, Avantium). Typically, 50 mg of as-prepared catalyst was diluted with 100 mg nonporous silica gel (Davisil grade 646) and loaded into a quartz reactor (ID = 2 mm, OD = 3 mm, L = 300 mm). The silica diluent showed no catalytic activity in control experiments. Reactions were performed between 200 and 500 °C at nominal atmospheric pressure. All gases were purchased from Airgas. 5% propylene in Ar was used together with dry air, N_2 (UHP) and He (UHP) as the standard. Propylene:O_2 ratios were varied (1:1, 3:1 and 5:1) and total flow rates varied from 10 to 30 mL/min. Reactions were performed at a space velocity of 140–180 mol propylene/min mol Cu and a GHSV of 36,200 mL/gcat/h. The effluent of each reactor was analyzed sequentially by a gas chromatograph (7890B, Agilent Technologies), equipped with a thermal conductivity detector (TCD) and 2 flame ionization detectors (FID). A simplified reaction diagram is presented in Scheme 1. However, methanol, ethanol, propanal, 1- and 2-propanol,

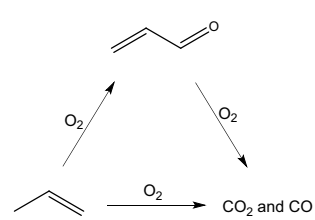

Scheme 1 Reaction scheme of propylene oxidation to acrolein or CO_x

propionic acid, acetaldehyde and propylene oxide were also detected in small quantities. Selectivities were calculated on a C_3 basis.

2.7 Microreactor Studies

Microreactor experiments were used for kinetic studies and long-term testing to evaluate catalyst deactivation. Propylene oxidation to acrolein was performed at atmospheric pressure in a packed-bed quartz microreactor. Typically 50 mg catalyst, previously calcined at 400 °C for 4 h in air, was diluted in 100 mg non-porous silica gel to achieve a bed height of 2–3 mm to minimize pressure and temperature gradients. The silica diluent showed no catalytic activity in control experiments. Catalysts were pre-treated at 250 °C with 33 mL/min of 6% O_2/balance He for 30 min to remove residual water before reaction and cooled to 200 °C. The temperature was ramped in 25 °C intervals up to 400 °C. The catalyst was held at each intermediate temperature for approximately 1 h. Reactions were performed at a constant space velocity of 14.2 mol propylene/min mol Cu, a total flow rate of 33 mL/min, and a GHSV of 39,600 mL/gcat/h. The ratio of propylene:O_2 was 1:1. Products were analyzed using an Agilent GC 6890 with FID and TCD in parallel. Instantaneous turnover frequencies for each GC injection are calculated from the differential region of product yield divided by contact time, and selectivities were calculated as shown below:

$$S_{C3} = \frac{Acrolein}{Acrolein + CO_2/3 + \frac{CO}{3} + C6\text{-}olefin \times 2}$$

3 Results and Discussion

3.1 Selection of Propylene:O_2 ratio and Active Metal in M/TMS-SiO_2 (M = Fe, Co, Cu)

Initial experiments were undertaken with CuO_x, FeO_x, and CoO_x supported on TMS-SiO_2 at target metal loadings of 1.0 and 0.1 metal atoms/nm^2. The initial catalyst testing was carried out on a 16-reactor parallel fixed bed reactor system to identify propylene to oxygen ratio. The ratio of propylene to O_2 was first investigated using 0.1 and 1.0 Cu atoms/nm^2; results of these experiments indicate that lower substrate-to-oxidant ratios favor acrolein selectively (Fig. S3). A ratio of propylene:O_2 to 1:1 was then chosen.

Figure 1a–c shows a comparison of the catalytic activity of FeO_x, CoO_x and CuO_x catalysts on TMS-SiO_2 at two different loadings measured at temperatures between 200 and 500 °C. The experiments revealed, as expected, increasing conversion of propylene with increasing temperature; however, increasing temperature generally led to increasing yields of CO_2 (i.e., complete oxidation of propylene) with limited selectivity for acrolein. Propylene conversion is lowest with the use of CoO_x systems, and while appreciable conversions were also observed for FeO_x systems, CuO_x was clearly the best-performing among the three metals chosen in this study in terms of selectivity to acrolein. In contrast, FeO_x and CoO_x systems favored deep oxidation products such as CO and CO_2. Furthermore, our data is consistent with previous literature reports that lower metal loadings improve the selectivity to partial oxidation at any given conversion, most likely due to more dispersed active sites [8]. While Cu loadings of 0.1 atom/nm^2 lead to lower conversion compared to 1 atom/nm^2 at low temperature, it is worth noting that higher conversion is achieved at 500 °C. The highest acrolein yield, 4.8% was obtained for 0.1 Cu at 400 °C at 36,000 mL/gcat/h. We note for 1 atom/nm^2 Cu that propylene conversion failed to increase with increasing temperature (i.e. conversions at 400 and 500 °C) which is indicative of deactivation via agglomeration of the CuO_x sites. TEM shows significant agglomeration of CuO_x in these materials (see Fig. S4), and this will be discussed further below. DR UV–Vis analyses of Cu- and Fe-based TMS-SiO_2 confirm a lesser degree of agglomeration for the samples at low loadings after reaction at various temperatures (Fig. S5). It should also be noted any deactivation with TOS is convoluted in with all this activity data, which can limit the quantitative utility of the rates determined from high-throughput screening. Nevertheless, this screening does allow for qualitative comparisons of large numbers of catalysts. Based on the higher selectivity seen in these initial results, we narrowed our scope to low loadings of CuO_x/SiO_2.

3.2 Effect of CuO_x on TMS-SiO_2 versus CuO_x on M–SiO_2 (M = Zr, Zn, V, Cr, Co)

To further enhance the activity of CuO_x catalysts and compare the effect of TMS capping with that of doping, we synthesized CuO_x on doped-SiO_2 with a variety of promoters. Promoter ions were chosen based on two hypotheses. Redox-active, oxophilic promoters (V, Cr, Co) may facilitate oxidant transfer from the active metal site by weakening the active metal–oxygen bond and acting as a chemical promoter. Alternately, promoter ions (Zr, Zn) that are more acidic than silanols may be better able to anchor the active CuO_x domain, thus improving catalyst stability against aggregation and other structural changes [35].

Figure 2 summarizes the results of the evaluation of a series of CuO_x/M-SiO_2 (0.05 to 0.25 Cu atoms/nm^2, M = Zr, V, Cr, Co, Zn) catalyst candidates for propylene oxidation to acrolein at 250 °C. With the notable exception of CuO_x/Zr–SiO_2, acrolein yields decreased with CuO_x loading due to rapidly decreasing selectivity to acrolein. At a low loading of 0.05 Cu atoms/nm^2, the trend in acrolein per-pass yield was:

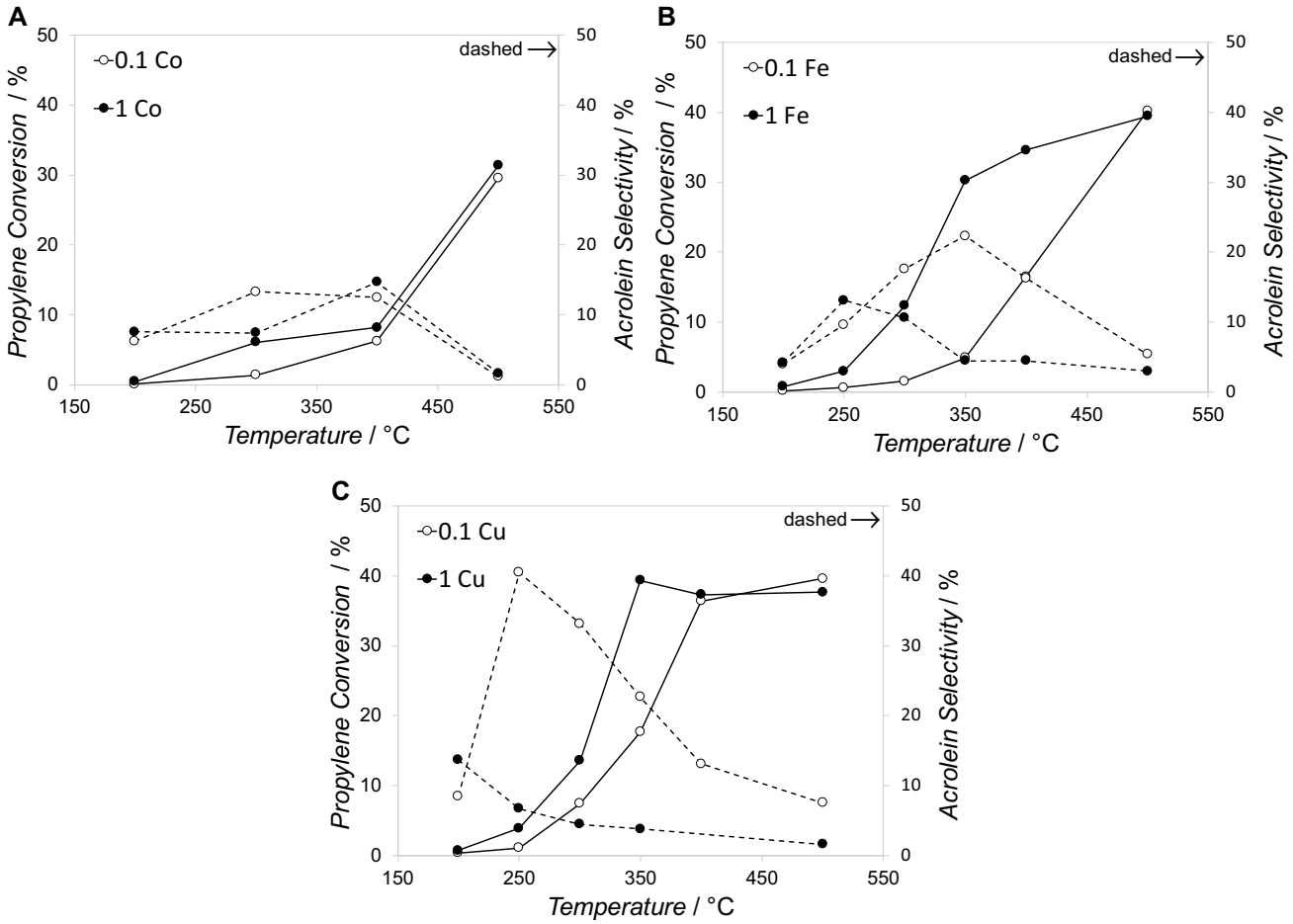

Fig. 1 Comparison of propylene conversions and acrolein selectivities of catalytic systems with target loadings of 0.1 and 1 Co (**a**), Fe (**b**) or Cu (**c**) atoms/nm^2 onto TMS-SiO_2 supports as a function of temperature (50 mg catalyst, propylene:O_2 1:1)

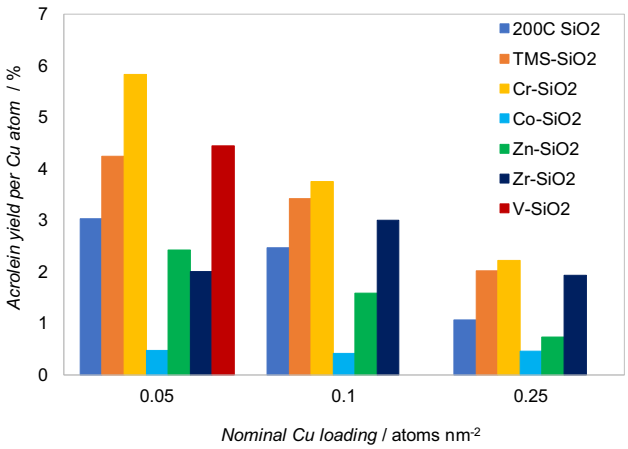

Fig. 2 Acrolein yield per Cu atom as a function of Cu loadings for Cu onto various supports (SiO_2, TMS-SiO_2, Cr–, Co–, Zn–, Zr–, and V–SiO_2). (50 mg catalyst, propylene: O_2 1:1, 250 °C)

CuO_x/Cr–SiO_2 > CuO_x/V–SiO_2 > CuO_x/TMS-SiO_2 > CuO_x/SiO_2 > CuO_x/Zn–SiO_2 > CuO_x/Zr–SiO_2 > CuO_x/Co–SiO_2. It can be noted that CuO_x/TMS-SiO_2 gives a higher acrolein yield compared to CuO_x on bare SiO_2 (vacuum treated at 200 °C), which indicates that a higher site isolation is favorable for the production of acrolein.

Following screening, the two of the highest-performing promoted catalysts (CuO_x/Cr–SiO_2 and CuO_x/V–SiO_2) as well as CuO_x/Zr–SiO_2 were selected for more detailed studies in a microreactor. Loadings of Cu and the promoters are presented in Table 1.

Activity and selectivity (to acrolein) data collected from the micro-reactor study are presented in Fig. 3. Data points represent an average over 60 min time on stream at a given temperature. Materials prepared with just the promoter ion and no copper (V–, Cr–, or Zr–SiO_2) were not as active as the heterobimetallic catalysts (Table 2, Fig. S6). Total propylene conversion reached as high as 32% under these conditions, and conversion rates normalized to the total amount of catalyst are reported in Fig. 3a. The most

Table 1 Characteristics of $CuO_x/M\text{-}SiO_2$ materials selected for microreactor studies

Catalyst	M (wt%)	Cu (wt%)	Cu (μmol/g_{cat})	Cu (atoms/nm^2)
CuO_x/SiO_2	–	0.45	70	0.085
$CuO_x/Zr–SiO_2$	3.40	0.47	75	0.090
$CuO_x/Cr–SiO_2$	0.70	0.45	69	0.082
$CuO_x/V–SiO_2$	2.37	0.35	55	0.066

prevalent products were CO and CO_2, not shown here. There were no significant side products formed, although dimerization products were observed in small quantities at low temperatures. The catalysts displayed linear Arrhenius behavior under differential conversion conditions (325 °C and below) (Fig. 3c). Acrolein yield and apparent activation energies are reported in Table 2.

Of the materials studied, $CuO_x/Cr–SiO_2$ displayed the highest overall propylene conversion at temperatures above 300 °C (Fig. 3a). However, the acrolein yield of $CuO_x/Cr–SiO_2$ is roughly equal to the sum of the acrolein yield of CuO_x/SiO_2 and $Cr–SiO_2$ (Table 2), so there is no evidence of synergistic interaction between CrO_x and CuO_x. Alternatively, although $CuO_x/Zr–SiO_2$ had higher propylene conversion than $CuO_x–SiO_2$, the yield of acrolein is less than that of the un-promoted copper catalyst. The addition of Zr lowers the selectivity of the catalyst to acrolein by disproportionately increasing the rate of formation of CO_2. Finally, $CuO_x/V–SiO_2$ maintained its selectivity to the desired acrolein product as temperatures increased, and above 300 °C, it had the highest selectivity, (Fig. 3b, d), and the highest rate of acrolein production. Moreover, the acrolein yield was higher than that of $CuO_x–SiO_2$ and $V–SiO_2$ combined, suggesting that synergistic effect exists between Cu and V. The acrolein yield obtained at 400 °C for $CuO_x/V–SiO_2$ was 3.4%, which is higher compared to that obtained from other Cu/V systems [24, 25]. When comparing with precious metal-free Cu-based catalyst [36], it is also in the same range as the one reported by Tüyüz et al. 3.7% [8] but they used a smaller GHSV (15,000 mL/gcat/h at the same O_2:C = 1:1), while we use almost 40,000 mL/gcat/h.

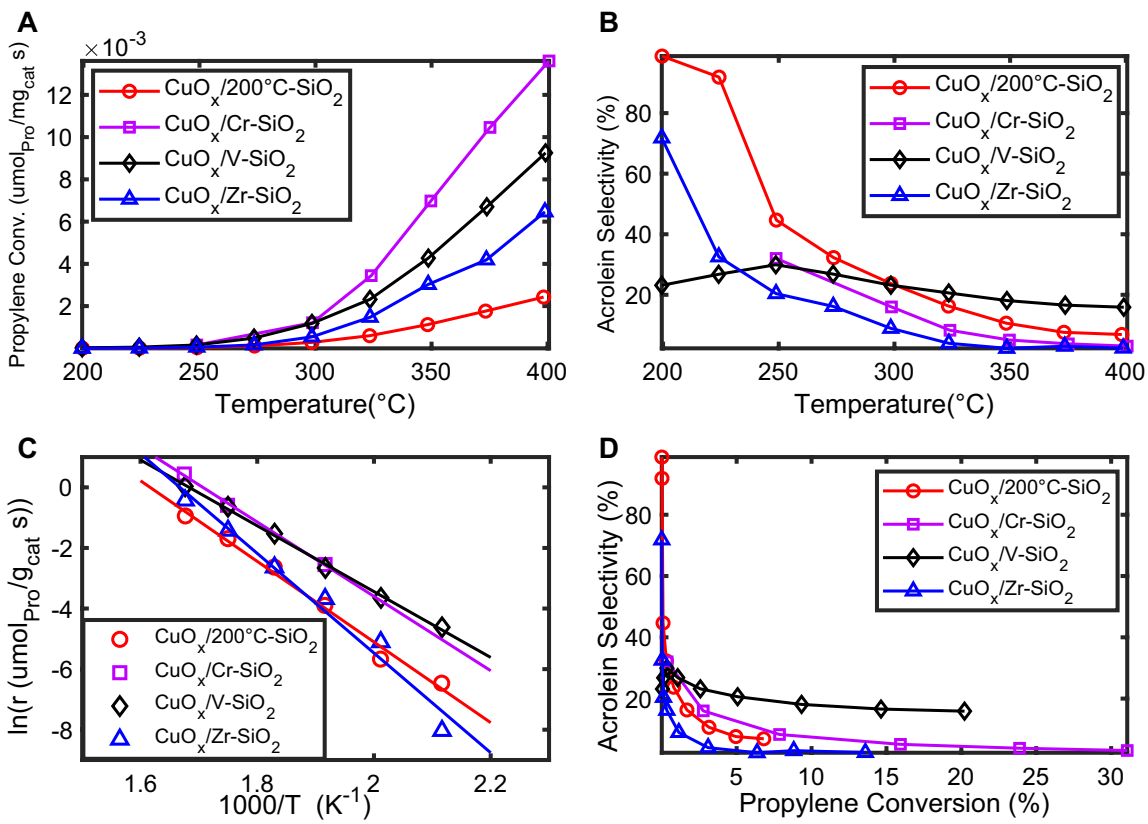

Fig. 3 Performance comparison of the promoted and unpromoted catalysts listed in Table 1. **a** Rate of propylene conversion normalized to catalyst mass at increasing temperatures, **b** Selectivity to acrolein on a C3 basis at increasing temperatures, **c** Arrhenius plot of rate of propylene conversion of copper supported on modified and unmodified silica, **d** Selectivity to acrolein at increasing extents of propylene conversion

Table 2 Rates of acrolein production and apparent activation energy for M–SiO_2 and CuO_x/M–SiO_2 materials (M = Cr, V and Zr)

Catalyst	$E_{A,app}$ (kJ/mol)	Acrolein yield ($\mu mol_{Acr}/mg_{cat}s \times 10^3$) 200 °C	300 °C	400 °C
CuO_x/SiO_2	98	1.1	33	82
CuO_x/Zr–SiO_2	137	0.19	17	56
CuO_x/Cr–SiO_2	86	< 0.01	90	190
CuO_x/V–SiO_2	90	23	120	660
Zr–SiO_2	92	< 0.01	3	38
Cr–SiO_2	47	9.4	55	120
V–SiO_2	102	2	27	240

Micro-reactor studies were also used to provide more insight into the deactivation of the high-performing catalysts. All of the materials tested showed a gradual deactivation and decrease in conversion (Fig. S7) and in the formation of CO_2 with time on stream for isotherms at or above 300 °C (Fig. 4a). However, the yield of acrolein remained nearly constant with time on stream (Fig. 4b). This finding suggests that at high temperatures, the rearrangement of metal oxides on the silica surface results in a decrease in the number of sites that are active for combustion while sites that are responsible for selective oxidation are preserved or possibly even generated.

3.3 CuO_x/M-SiO_2 Characterization Pre- and Post-Catalysis (M = Zr, V, Cr)

The Raman spectra of the as-prepared catalysts (0.05 CuO_x/SiO_2, Cr–SiO_2, V–SiO_2, Zr–SiO_2, 0.05 CuO_x/Cr–SiO_2, 0.05 CuO_x/V–SiO_2 and 0.05 CuO_x/Zr–SiO_2) as well as bulk CuO, monoclinic ZrO_2, SiO_2 and V_2O_5/SiO_2 are presented in Fig. 5. In agreement with previous reports, features at 296 and 345 and 660 cm^{-1} are observed for bulk crystalline CuO reference sample [37]. In the case of CuO_x/SiO_2, CuO_x/Cr–SiO_2, CuO_x/V–SiO_2 and CuO_x/Zr–SiO_2, there is a vibration around 976 cm^{-1} that is not observed in the bulk phase

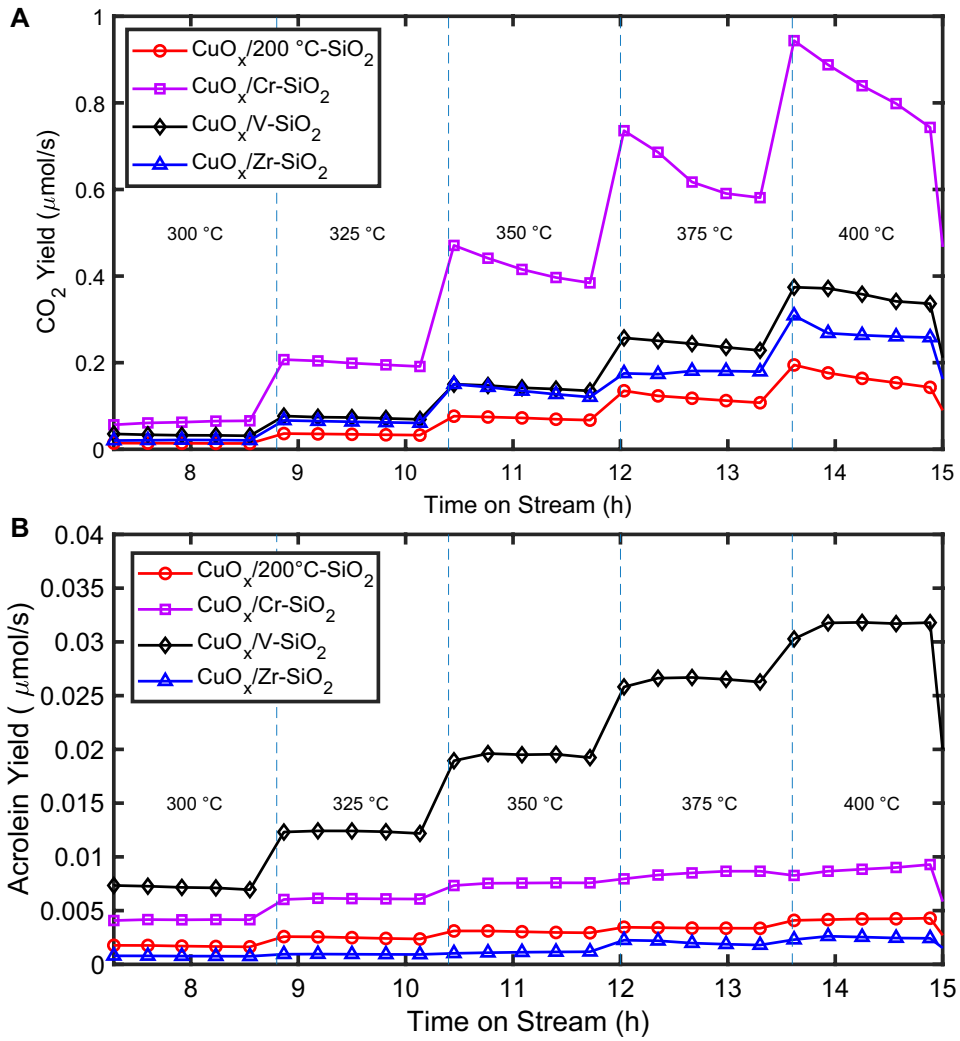

Fig. 4 Comparison for catalytic systems with nominal loading of 0.05 Cu atoms/nm^2 onto various supports of **a** CO_2 and **b** acrolein yield with time on stream. Propylene conversion is shown in Fig. S7

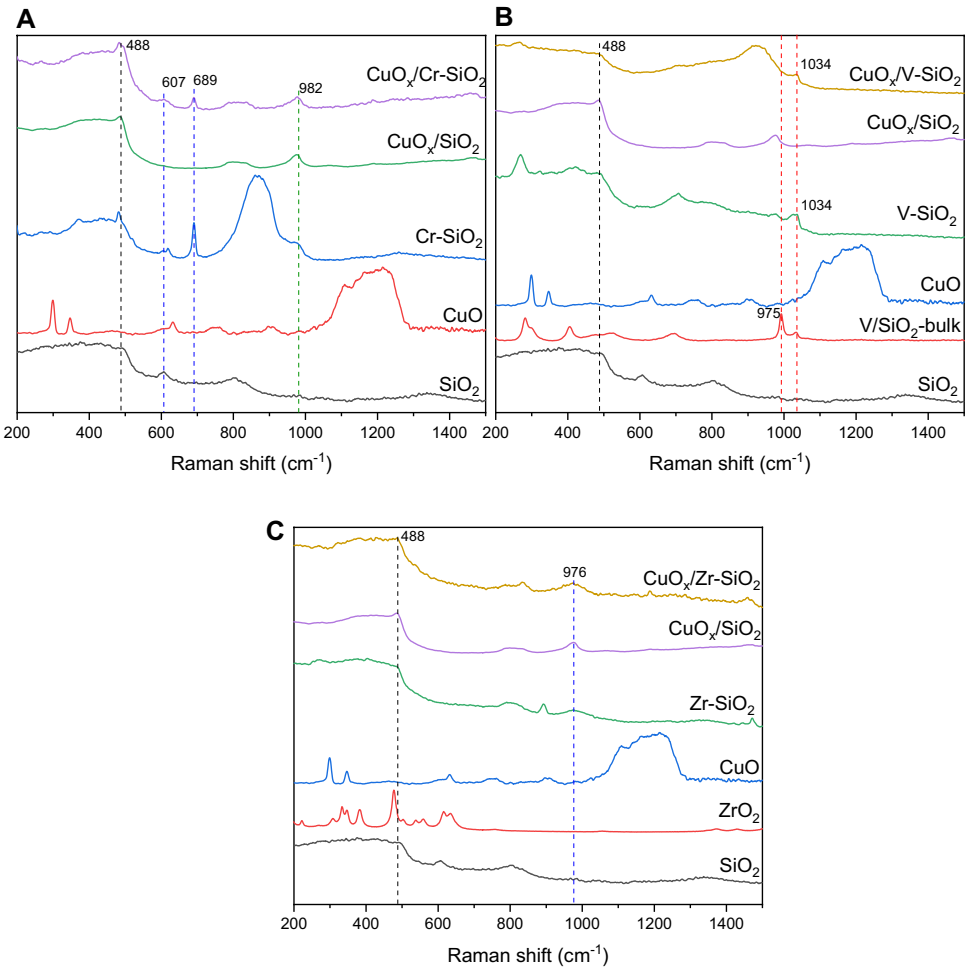

Fig. 5 Raman spectra of as-prepared Cr–SiO_2, 0.05 CuO_x/SiO_2 and 0.05 CuO_x/Cr–SiO_2 **a**, V–SiO_2, 0.05 CuO_x/SiO_2 and 0.05 CuO_x/V–SiO_2 (**b**) and Zr–SiO_2, 0.05 CuO_x/SiO_2 and 0.05 CuO_x/Zr–SiO_2 (**c**). Reference spectra of SiO_2, ZrO_2, CuO, and V_2O_5/SiO_2 added for comparison

of CuO, but is due to silica aerogel [38, 39]. For Cr–SiO_2, the Raman spectrum is dominated by one strong, broad band at 890 cm^{-1} and shoulders around 982, and 689 cm^{-1}. The band at 890 cm^{-1} is typical for dichromate [40]. The Raman band at around 982 cm^{-1} is characteristic of a dehydrated chromium oxide species [41, 42]. However, previous Raman studies concluded that this chromium oxide specie is predominantly present as a polychromate specie [40]. An interesting observation was that the peak around 689 cm^{-1} observed in the binary and ternary chromium systems is not observed in the literature [40, 42–44] for reported Cr–SiO_2 catalysts. However, no isolated surface chromate species were observed (Cr=O vibrations at 1030 cm^{-1}). On CuO_x/Cr-SiO_2, the large peak at 890 cm^{-1} disappears and the vibration at 689 cm^{-1} dampens. The presence of polychromate species in CuO_x/Cr–SiO_2 may explain the high conversion of propylene into CO_2, as seen in Fig. 4a. For vanadium based catalysts a vibration was found at 1034 cm^{-1} characteristic of molecularly dispersed 2D V=O [44, 45]. The absence of 995 cm^{-1} vibration (3D V=O) [45] in comparison with bulk V_2O_5 indicates the V–SiO_2 is well-dispersed.

Since the partial oxidation reaction follows a redox mechanism, the reducibility of the samples, was investigated by the temperature-programmed reduction (TPR) technique. The TPR profile of the 0.05 CuO_x/SiO_2, Cr–SiO_2, 0.05 CuO_x/Cr–SiO_2, V–SiO_2, 0.05 CuO_x/V–SiO_2, Zr–SiO_2 and 0.05 CuO_x/Zr–SiO_2 after treatment in air at 500 °C are shown in Fig. S8. There is a small peak at 252 °C for CuO_x/SiO_2 which corresponds to highly dispersed CuO and a broad peak up to 630 °C which corresponds to dispersed Cu (II) species onto silica which is hard to reduce [46, 47]. There is one main sharp peak for Cr–SiO_2 and for V–SiO_2 while for Zr–SiO_2, there is one broad peak. For V–SiO_2, the peak reduction temperature is at 568 °C, which does correspond to either isolated or oligomeric VO_x species in p-tetrahedral and square-pyramidal coordination [48]. The peak at 463 °C for Cr–SiO_2 corresponds to the reduction of Cr(VI) to Cr_2O_3 [49]. The temperature for reduction of these promoter oxides are lowered in the presence of copper indicating close interactions, as reported for various loadings of Cu onto V-HMS [50]. In addition, for CuO_x/V–SiO_2, the copper species reduce at higher temperature indicating a stronger interaction of Cu with vanadium than Cu with the

SiO_2 support. This may explain the enhanced stability of copper species when supported on V–SiO_2. In addition the hydrogen consumption is enhanced for copper species on V–SiO_2, which also indicates more lattice oxygen is available which is responsible for the enhanced reactivity of allyl oxidation [47].

Analysis of the spent CuO_x/SiO_2 catalysts (from microreactor studies) via DR UV–Vis provided a rationale for the differences in the effects of various promoters (Fig. 6). The spent CuO_x/SiO_2 catalyst displays increased absorption > 350 nm, consistent with aggregation to form extended CuO sheets, and > 550 nm indicative of aggregation to form larger CuO crystallites [51, 52], as compared to the spectra after preliminary calcination. The CuO_x/Cr–SiO_2 and CuO_x/Zr–SiO_2 show slightly increased absorption between 350 and 550 nm consistent with some growth of CuO sheets. In contrast, CuO_x/V–SiO_2 catalysts do not display increased absorption > 350 nm which indicates the discrete VO_x phases particularly stabilize a highly dispersed CuO phase [53]. It should be acknowledged that CrO_x and VO_x both contribute to the total absorption spectra in addition to CuO_x, which may obscure precisely which domains are changing under reaction conditions.

PDF characterization of the local structure of calcined (400 °C) CuO_x/M–SiO_2 systems was carried out in order to elucidate structural factors responsible for the stability of CuO_x. Positions of maxima correspond directly to interatomic distances; while areas are related to coordination numbers. Figure 7 shows the data for the calcined samples. Some of the interatomic distances do not correspond to CuO, Cu_2O or Cu^0, for instance 2.7, 4.0, 5.3 and 5.9 Å but could

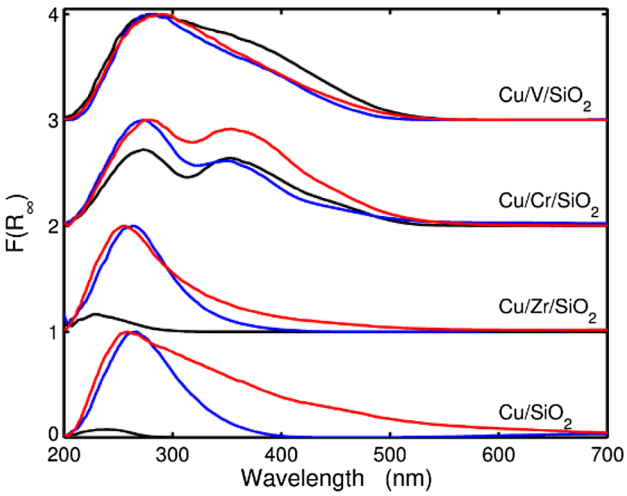

Fig. 6 Absorption spectra of 0.05 CuO_x/SiO_2 and CuO_x/M–SiO_2 (M = V, Cr, and Zr) catalysts. M–SiO_2 (black), freshly calcined (400 °C 4 h air) 0.05 CuO_x/M-SiO_2 (blue) and after microreactor studies (red). Spectra are normalized to freshly calcined CuO_x/M-SiO_2. LMCT maximum for comparison

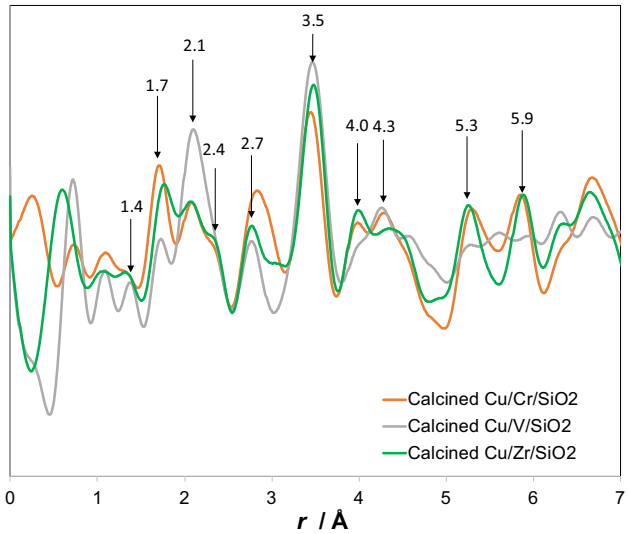

Fig. 7 Differential pair distribution data for the calcined samples (SiO_2 data was subtracted.)

be attributed to deformation of the strained CuO structure indicating highly dispersed CuO phase onto support [54]. The main peak at 3.5 Å can also be attributed to Cu–O–M for instance in $Cu_2[\mu\text{-}(\eta^2{:}\eta^2\text{-}O_2)]$, in agreement with a previous report by Vilella and co-workers on the stability of oxo-bridged Cu species supported on zeolites [55]. The calcined CuO_x/V–SiO_2 has short range ordered features, while the CuO_x/Cr–SiO_2 and CuO_x/Zr–SiO_2 show well defined peaks to longer distance, which supports the better stability of CuO_x/V–SiO_2 against formation of aggregates.

The stabilizing effect of a promoter can also be confirmed visually via TEM. Figure 8 compares TEM images of post-catalysis CuO_x/SiO_2 and CuO_x/V–SiO_2 (Fig. 8b, c). On CuO_x/SiO_2 there is evident formation of crystalline CuO_x phases larger than 10 nm in diameter. TEM images of as-prepared V–SiO_2 (Fig. 8a) showed the presence of clusters of less than 5 nm. Raman (Fig. 5) confirmed these clusters to be 2D V=O. Post-catalysis CuO_x/V–SiO_2 maintains these VO_x islands and there is no evidence of CuO_x or VO_x aggregating further, which is also in agreement with the DR UV–Vis (Fig. 6). This is consistent with microreactor studies in which the CuO_x/V–SiO_2 undergoes less deactivation over the course of reaction than CuO_x/Cr–SiO_2 and CuO_x/Zr–SiO_2 or (non-promoted) CuO_x/SiO_2 catalysts (see Fig. S7). On the other hand, the Zr–SiO_2 likely does not stabilize the CuO_x phase well due to its poor dispersion leaving large areas of SiO_2 surface without ZrO_x to stabilize the CuO_x phase (Fig. S11), which is consistent with increased absorption > 350 nm (Fig. 6) indicative of sintering of the CuO_x phase during reaction on the CuO_x/Zr–SiO_2 catalyst. It is possible that the increased absorption in the tail is due

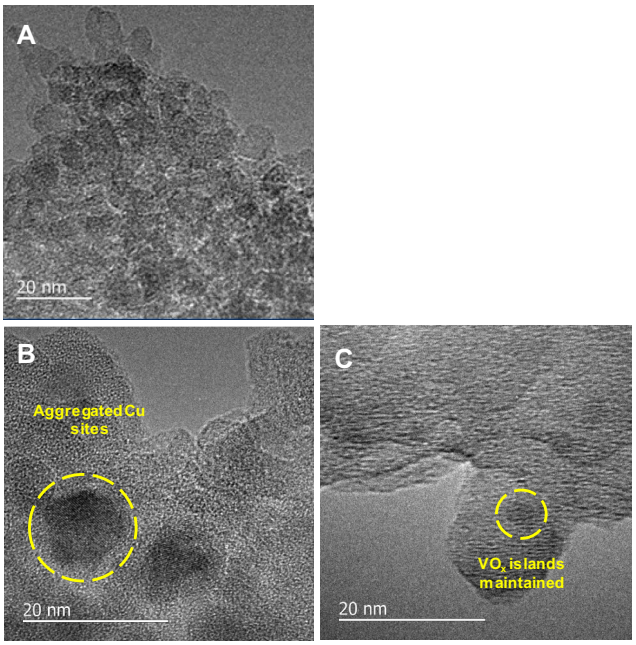

Fig. 8 TEM images of as-prepared V–SiO_2 (**a**), post-catalysis of CuO_x/SiO_2 (**b**) and CuO_x/V–SiO_2 (**c**)

to sintering of CuO_x that sits directly on the SiO_2 support rather than ZrO_2 crystallites.

Several literature reports on selective oxidation also report CuO_x promotion and stabilization by VO_x or CrO_x. Yang and co-workers reported synergistic effects between copper and vanadium, attributing the increase in catalytic epoxidation of propylene by oxygen to enhanced dispersion of copper by vanadium [23]. In a separate work, Bøyesen and others also identified a synergistic Cu/V redox pair prepared via co-deposition into AlPO-5 with selective formation of acrolein from propylene oxidation as a result of extralattice oxygens generated by reactive Cu/V pairs linked by bridging oxygens (Cu–O–V) [24–26]. Dekker and co-workers also reported the CO oxidation by O_2 and N_2O using Cu–Cr/Al_2O_3 by co-impregnation from an aqueous solution of Cu(II) and Cr(III) nitrate, with Cr thought to stabilize Cu against sintering by limiting Cu reduction via the formation of a $CuCr_2O_4$ phase [29]. This promoter effect of Cr on Cu via a $CuCr_2O_4$ spinel was previously reported by Khanmamedov's group in their studies of Al–Cu–Cr catalysts for H_2S and CO oxidation [30].

4 Conclusions

Highly dispersed silica-supported catalysts were studied for their activity, selectivity, and stability in catalyzing the selective oxidation of propylene to acrolein. High active site dispersion, could be achieved via two general synthetic strategies, which included (i) the decrease in SiO_2 surface hydroxyl concentration via covalent surface modification (silanol capping), or (ii) the modification of the oxide surfaces with cationic 'anchors' that stabilize highly dispersed catalytic sites. In a first part, a series of highly dispersed metal (Fe^{3+}, Co^{2+}, Cu^{2+}) sites on trimethylsilyl-capped SiO_2 via solution-phase synthesis was tested. Evaluation of catalyst candidates reveals minimal activity of CoO_x/SiO_2 catalysts while FeO_x/SiO_2 systems produced more of undesirable deep oxidation product, CO_2. Appreciable propylene conversion and selectivity for acrolein were observed for CuO_x/SiO_2 systems which, however, suffered from rapid deactivation due to CuO_x agglomeration under reaction conditions. The second part included synthesizing a series of highly dispersed copper of various surface densities, onto modified-SiO_2 with promoters (V, Cr, Zn, Co, Zr). Several promising promoters, V and Cr, were identified and subjected to more rigorous activity and durability testing. CuO_x/V–SiO_2 was ultimately the catalyst with the highest acrolein yield. Across a range of temperatures, the yield was much higher than the combined yield of CuO_x/SiO_2 and control VO_x/SiO_2 catalysts, suggesting a synergistic effect between the two metals that was not observed for any other promoter. Although all of the materials tested showed a gradual decrease in total propylene conversion at high temperatures, the majority of the observed deactivation came from a decrease in CO_x production. Acrolein selectivity remained nearly constant and even improved for both CuO_x/V–SiO_2 and CuO_x/Cr–SiO_2, which implies that at high temperatures, the rearrangement of metal oxides on the silica surface results in a decrease in the number of sites that are active for combustion while the sites that are responsible for selective oxidation are preserved. Finally, it was seen via Raman, TPR-H_2, DR UV–Vis, PDF and TEM that one potential reason for the high activity and stability of CuO_x/V–SiO_2 is that the addition of V, which formed 2D islands, appears to help minimize the aggregation of CuO_x into large clusters before, during calcination and under reaction conditions.

Acknowledgements This work is supported by the Department of Energy, Laboratory Directed Research and Development funding at Argonne National Laboratory under Contract No. DE-AC02-06CH11357. This research used resources of the Advanced Photon Source and the Center for Nanoscale Materials, U.S. Department of Energy (DOE) Office of Science User Facilities operated for the DOE Office of Science by Argonne National Laboratory under Contract No. DE-AC02-06CH11357.

References

1. Belin S, Bracey CL, Briois V, Elllis PR, Hutchings GJ, Hyde TI, Sankar G (2013) Catal Sci Technol 3:2944–2957
2. Baussart H, Delobel R, Le Bras M, Leroy JM (1979) J Chem Soc, Faraday Trans 1(75):1337–1345

3. Liu CH, Lai NC, Lee JF, Chen CS, Yang CM (2014) J Catal 316:231–239
4. Imachi M, Kuczkowski RL, Groves JT, Cant NW (1983) J Catal 82:355–364
5. Choi HS, Lin JT, Kuczkowski RL (1986) J Catal 99:72–78
6. Horváth B, Soták T, Hronec M (2011) Appl Catal A 405:18–24
7. Albonetti S, Cavani F, Trifirò F (1996) Catal Rev 38(4):413–438
8. Tüysüz H, Galilea JL, Schüth F (2009) Catal Lett 131:49–53
9. Schuh K, Kleist W, Høj M, Trouillet V, Beato P, Jensen AD, Grunwaldt JD (2015) Catalysts 5(3):1554–1573
10. Zhai Z, Wütschert M, Licht RB, Bell AT (2016) Catal Today 261:146–153
11. Pudar S, Oxgaard J, Chenoweth K, van Duin ACT, Goddard WA (2007) J Phys Chem C 111:16405–16415
12. Fierro JLG, Gambaro LA, Cooper TA, Kremenić G (1983) Appl Catal 6:363–378
13. Panyad S, Jongpatiwut S, Sreethawong T, Rirksomboon T, Osuwan S (2011) Catal Today 174:59–64
14. Labaki M, Lamonier JF, Siffert S, Zhilinskaya EA, Aboukaïs A (2003) Coll Surf A 227:63–75
15. Inui T, Ueda T, Suehiro M (1980) J Catal 65:166–173
16. Grasselli RK (2002) Top Catal 21(1–3):79–88
17. Bettahar MM, Costentin G, Savary L, Lavalley JC (1996) Appl Catal A 145:1–48
18. Bracey CL, Carley AF, Edwards JK, Ellis PR, Hutchings GJ (2011) Catal Sci Technol 1:76–85
19. Wang X, Zhang Q, Guo Q, Lou Y, Yang L, Wang Y (2004) Chem Commun 1396:1397. https://doi.org/10.1039/B402839B
20. Krenzke LD, Keulks GW (1980) J Catal 61:316–325
21. Forzatti P, Villa PL (1982) J Catal 76:188–207
22. Allen M, Betteley R, Bowker M, Hutchings GJ (1991) Catal Today 9:97–104
23. Yang L, He J, Zhang Q, Wang Y (2010) J Catal 276:76–84
24. Bøyesen KL, Kristiansen T, Mathisen K (2014) Phys Chem Chem Phys 16:20451–20463
25. Bøyesen KL, Kristiansen T, Mathisen K (2015) Catal Today 254:21–28
26. Bøyesen KL, Mathisen K (2014) Catal Today 229:14–22
27. Wojciechowska M, Haber J, Łomnicki S, Stoch J (1999) J Mol Catal A 141:155–170
28. Xanthopoulou G, Vekinis G (1998) Appl Catal B 19:37–44
29. Dekker NJJ, Hoorn JAA, Stegenga S, Kapteijn F, Moulijn FA (1992) Am Inst Chem Eng J 38(3):385–396
30. Khanmamedov TK, Kalinkin AV, Kundo NN, Novopashina VM (1988) React Kinet Catal Lett 37(1):83–88
31. Keranen J, Guimon C, Liskola E, Auroux A, Niinisto L (2003) J Phys Chem B 107(39):10773–10784
32. Liu YM, Feng WL, Wang LC, Cao Y, Dai WL, He HY, Fan KN (2006) Catal Lett 106(3–4):145–152
33. Schweitzer NM, Hu B, Das U, Kim H, Greeley J, Curtiss LA, Stair PC, Miller JT, Hock AS (2014) ACS Catal 4:1091–1098
34. Hu B, Getsoian A, Schweitzer NM, Das U, Kim H, Niklas J, Poluektov O, Curtiss LA, Stair PC, Miller JT, Hock AS (2015) J Catal 322:24–37
35. Camacho-Bunquin J, Ferrandon M, Sohn H, Yang D, Liu C, Ignacio-de Leon PA, Perras FA, Pruski M, Stair PC, Delferro M (2018) J Am Chem Soc 140:3940–3951
36. Song W, Perez Ferrandez DM, van Haandel L, Liu P, Nijhuis TA (2015) hensen EJM. ACS Catal 5:1100–1111
37. Deng Y, Handoko AD, Du Y, Xi S, Yeo BS (2016) ACS Catal 6:2473–2481
38. Lgarashi K, Tajiri K, Tai Y, Tanemura S (1993) Suppl Z Phys D26:S207
39. Owens L, Tillotson TM, Hair IM (1995) J Non-Cryst Sol 186:177–183
40. Jehng JM, Wachs IE, Weckuysen BM, Schoonheydt RA (1995) J Chem Soc Faraday Trans 91(5):953–961
41. Kim DS, Tatibouet JM, Wachs IE (1992) J Catal 136:209–221
42. Weckhuysen BM, Wachs IE (1996) J Phys Chem 100:14437–14442
43. Strunk J, Bañares MA, Wachs IE (2017) Top Catal 60:1577–1617
44. Lee EL, Wachs IE (2007) J Phys Chem C 111:14410–14425
45. Xie S, Iglesia E, Bell AT (2001) J Phys Chem B 105:5144–5152
46. Niu X, Zhao T, Yuan F, Zhu Y (2015) Sci Rep 5:9153
47. Chu H, Yang L, Zhang Q, Wang Y (2006) J Catal 241:225–228
48. Arena F, Fruteri F, Parmaliana A (1999) Catal Lett 60:59–63
49. Bugrova TA, Litvyakova NN, Mamontov GV (2015) Kinet Catal 56(6):746–752
50. Hu L, Yue B, Chen X, He H (2014) Catal Commun 43:179–183
51. Nauert SL, Schax F, Limberg C, Notestein JM (2016) J Catal 341:180–190
52. Barton DG, Shtein M, Wilson RD, Soled SL, Iglesia E (1999) J Phys Chem B 103:630–640
53. Gao X, Wachs IE (2000) J Phys Chem B 104:261–1268
54. Pakharukova VP, Moroz EM, Zyuzin DA, Ishchenko AV, Dolgikh LY, Strizhak PE (2015) J Phys Chem C 119:28828–28835
55. Vilella L, Studt F (2016) Eur J Inorg Chem 2016:1514–1520

Affiliations

Patricia Anne Ignacio-de Leon[1] · Magali Ferrandon[2] · Louisa M. Savereide[3] · Scott L. Nauert[3] · Jorge Moncada[4] · Rachel Klet[2] · Karena Chapman[5] · Massimiliano Delferro[2] · Jeffrey Camacho-Bunquin[2] · Carlos A. Carrero[4] · Justin M. Notestein[3] · SonBinh Nguyen[6]

Justin M. Notestein
j-notestein@northwestern.edu

[1] Advanced Materials Division, Argonne National Laboratory, Argonne, IL 60439, USA

[2] Chemical Sciences and Engineering Division, Argonne National Laboratory, Argonne, IL 60439, USA

[3] Department of Chemical and Biological Engineering, Northwestern University, Evanston, IL 60208, USA

[4] Department of Chemical Engineering, Auburn University, Auburn, AL 36849, USA

[5] X-ray Sciences Division, Advanced Photon Source, Argonne National Laboratory, Argonne, IL 60439, USA

[6] Department of Chemistry, Northwestern University, Evanston, IL 60208, USA